

Rise of the Andes

Carmala N. Garziona,^{1*} Gregory D. Hoke,¹ Julie C. Libarkin,² Saunia Withers,³ Bruce MacFadden,⁴ John Eiler,⁵ Prosenjit Ghosh,⁶ Andreas Mulch⁷

The surface uplift of mountain belts is generally assumed to reflect progressive shortening and crustal thickening, leading to their gradual rise. Recent studies of the Andes indicate that their elevation remained relatively stable for long periods (tens of millions of years), separated by rapid (1 to 4 million years) changes of 1.5 kilometers or more. Periodic punctuated surface uplift of mountain belts probably reflects the rapid removal of unstable, dense lower lithosphere after long-term thickening of the crust and lithospheric mantle.

The surface uplift of mountain belts, such as the central Andes plateau, has long been thought to be the isostatic response of shortening and thickening of the continental crust. Recently developed isotopic techniques allow us to determine the uplift history of the central Andes independently from the shortening history. These results show that shortening and uplift are temporally decoupled, with shortening and thickening happening over protracted periods of time, whereas uplift occurs geologically rapidly. Thus arises a paradox: Why does slow, continuous shortening and thickening not produce slow, continuous isostatic uplift in the central Andes?

Both crustal thickening and the removal of relatively dense mantle or lower crust can generate isostatic surface uplift (1, 2). Paleoelevation studies help resolve the geodynamic evolution of mountain belts because the rate and lateral extent of surface uplift depends on the processes involved. Here, we synthesize the elevation history of the central Andes, Earth's second largest mountain belt. We then compare paleoelevation estimates to histories of regional incision, sedimentation, shortening, and volcanism within the mountain belt to characterize lithospheric evolution and the geodynamic mechanisms that led to surface uplift.

The central Andean plateau (Fig. 1), with a width of ~400 km and an average elevation of ~4 km, is a typical example of an active plate margin where oceanic lithosphere is subducted beneath continental lithosphere. At its widest, the central Andean plateau consists of the internally drained Altiplano basin at an elevation of ~3800 m that is bounded by the Western and Eastern Cordilleras, where peak elevations exceed 6 km. The Western Cordillera is a chain of volcanic edifices

¹Department of Earth and Environmental Sciences, University of Rochester, Rochester, NY 14627, USA. ²Department of Geological Sciences, Michigan State University, East Lansing, MI 48824, USA. ³Department of Plant Biology, Michigan State University, East Lansing, MI 48824, USA. ⁴Florida Museum of Natural History, University of Florida, Gainesville, FL 32611, USA. ⁵Division of Geological and Planetary Sciences, California Institute of Technology, Pasadena, CA 91125, USA. ⁶Center for Atmospheric and Oceanic Science, Indian Institute of Science, Bangalore, 560 012, India. ⁷Institut für Geologie, Universität Hannover, 30167 Hannover, Germany.

*To whom correspondence should be addressed. E-mail: garziona@earth.rochester.edu

associated with the modern Andean magmatic arc, whereas the Eastern Cordillera and Altiplano basin record a history of folding and faulting. The central Andes have a protracted crustal shortening history spanning the last 50 million years (My) (3–5) that has generated crustal thicknesses of ~70 km below the highest topography in the Eastern and Western Cordillera and 60 to 65 km below the central Altiplano (6). Geophysical observations suggest that eclogitic lower crust is absent beneath much of the plateau (6). The mantle between 16°S and 20°S shows the lowest *P* wave velocities below the Altiplano/Eastern Cordillera transition, suggesting that virtually all of the mantle lithosphere has been

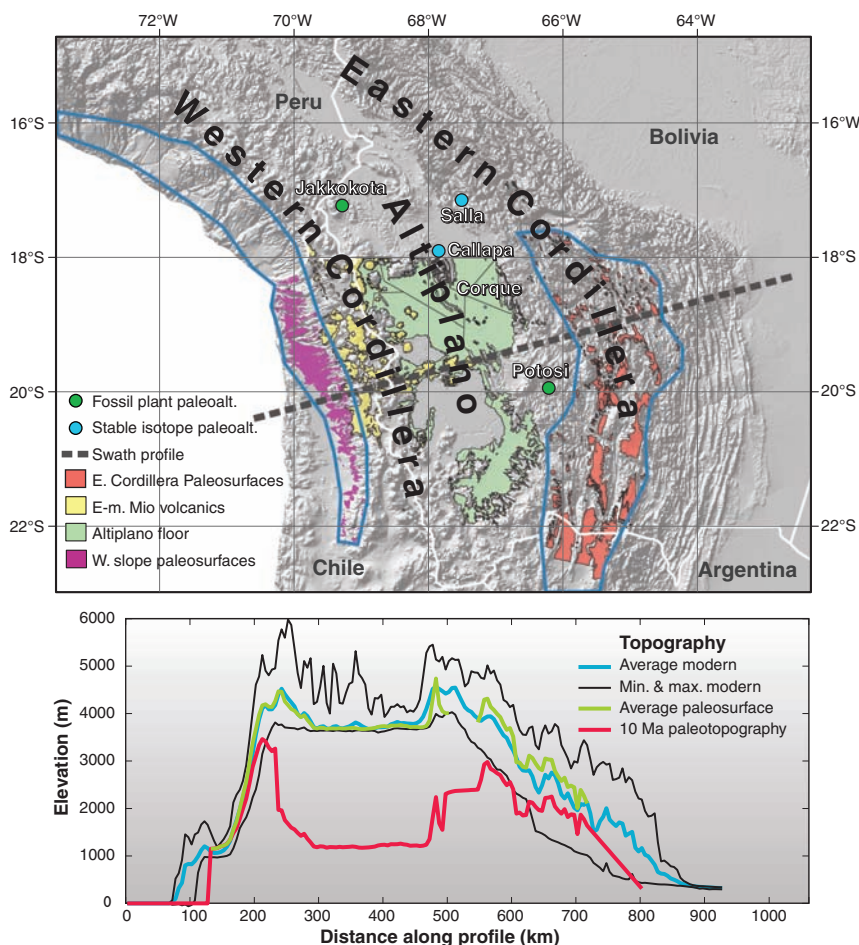


Fig. 1. Elevations of the Central Andean plateau based on Shuttle Radar Topography Mission 30 data and modern versus 10 Ma paleotopography profiles. (**Top**) Shaded relief topography of the central Andean plateau between 17.5°S and 23°S with colored areas representing the different paleosurface data used to reconstruct the topography of the Andes at 10 Ma. Regions outlined in blue show low-relief paleosurfaces that underwent rotation and incision beginning in late Miocene time. Green dots denote locations of Miocene paleobotanical estimates of paleoelevation (20, 21). Blue dots indicate locations of late Miocene stable isotope paleoelevation and paleotemperature estimates shown in Fig. 2. The large gap between the pale green and red paleosurfaces corresponds to the Los Friales ignimbrite shield. The dashed line marks the center of a 100-km-wide swath average profile across the central Andean plateau. (**Bottom**) Profiles showing the modern maximum and minimum topography (thin black lines), the average modern topography (light blue), and the average topography of the areas identified as paleosurfaces (green). The red line represents the topography of the Andes at 10 Ma based on the paleoelevation estimates given in Fig. 4 (center of plateau) and river incision-based estimates of relief generation for the eastern and western flanks of the Altiplano. The data gap created by the Los Friales ignimbrite shield and the Subandes is filled by linear interpolations.

removed (7–9). In addition, high $^3\text{He}/^4\text{He}$ ratios in hydrothermal fluids and gases across much of the Altiplano and Eastern Cordillera indicate the degassing of mantle asthenosphere-derived magmas (10). Together, these observations support previous suggestions for the southern Altiplano and Puna (11, 12) that both mantle lithosphere and eclogitic lower crust were removed below much of the Altiplano and the western part of the Eastern Cordillera (6). Removal of lower lithosphere might occur rapidly by delamination or convective removal (1, 13) or gradually by ablative subduction of foreland cratonic lithosphere (14, 15). Either case results in an influx of lighter asthenosphere, generating surface uplift of several kilometers. However, rapid removal of lower lithosphere would result in surface uplift in as little as several million years, whereas gradual removal by ablative subduction would generate surface uplift over tens of millions of years, coincident with crustal shortening.

Climate Trends and Subsidence History

The Altiplano and Eastern Cordillera contain thick accumulations of Oligocene through late Miocene fluvial, floodplain, and lacustrine deposits (16). The oxygen ($\delta^{18}\text{O}$) and hydrogen (δD) isotopic composition of paleosol carbonates and authigenic clays from volcanoclastic units provide a record of meteoric water composition that is the basis for stable isotope paleoelevation estimates (Fig. 2). Stable carbon isotope ($\delta^{13}\text{C}$) values of paleosol carbonates provide a record of plant respiration rates that can be used as a proxy for aridity (i.e., lower plant respiration reflects a more arid climate). Depositional environments within a 3.6-km-thick succession preserved in the eastern limb of the Corque syncline include fluvial channel sandstones and floodplain mudstones in the lower 1.4 km and upper 700 m, as well as a widespread freshwater-to-playa lake system that can be traced more than 100 km along strike. Both sedimentology and carbon isotopes in this section suggest that the central Altiplano became more arid between ~10 and 6 million years ago (Ma) (17). Fluvial channel deposits decreased in thickness and lateral extent up-section, further suggesting a decrease in discharge. Over the same time interval, $\delta^{13}\text{C}$ values of pedogenic carbonates increased by ~3 per mil (‰), suggesting a decrease in plant-respired CO_2 (17). Despite evidence for increasing aridity, the $\delta^{18}\text{O}$ values of palustrine and paleosol carbonates ($\delta^{18}\text{O}_\text{c}$) decrease by ~3 ‰ (Fig. 2), a change opposite of the expected trend for higher rates of surface-water evaporation. More positive $\delta^{18}\text{O}$ values observed in the older part of the record are synchronous with observations of wetter conditions, suggesting that evaporative enrichment of ^{18}O is an unlikely cause for the trend to more negative $\delta^{18}\text{O}$ values over time.

Sedimentation rates in the Altiplano reflect rates of subsidence relative to the surrounding topography. Sedimentation rates in the central Altiplano and Puna dramatically decreased after 10 Ma (18) (Fig. 3). Between 13 and 9 Ma,

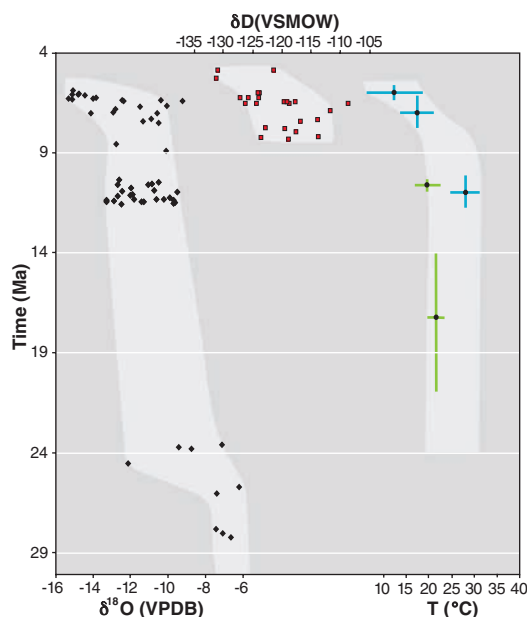


Fig. 2. Stable isotope paleoelevation proxies over time. $\delta^{18}\text{O}$ and δD values are from authigenic (paleosol and palustrine) carbonates and shallow groundwater cements. δD values are from authigenic clays in volcanic ash deposits. Paleotemperature estimates are derived from Δ_{47} measurements on pedogenic carbonates (22) (blue) and fossil-leaf physiognomy (20, 21) (green). Horizontal error bars reflect the 1σ variation on a group of pedogenic nodules. Vertical bars represent the age range (including uncertainty) of the sample group. VSMOW, Vienna standard mean ocean water; VPDB, Vienna Pee Dee belemnite.

sedimentation rates were extremely high, averaging 880 m/My (Fig. 3). During this time period, widespread lacustrine deposition suggests underfilled basin conditions. By 8.6 Ma, fluvial deposition resumed and subsidence decreased dramatically, averaging 0.12 mm/year.

Paleoelevation Constraints

Shallow marine deposits of the El Molino Formation require that the Altiplano lay at sea level at the end of Cretaceous time (19). Paleotemperature estimates derived from fossil-leaf physiognomy in the northern Altiplano and Eastern Cordillera (Fig. 1) suggest that paleoelevations were <1.3 km at ~15 to 20 Ma (20) and <2 km by ~10 Ma (21). Both the oxygen isotopic composition of rainfall and surface temperatures vary as a function of elevation. Stable oxygen isotope values of pedogenic carbonate and carbonate cement should reflect the composition of soil water and shallow groundwater, which is a reflection of rainfall composition and near surface temperature. The abundance of ^{13}C - ^{18}O bonds relative to a random distribution of carbon and oxygen isotopes in carbonate (measured by the Δ_{47} value of CO_2 extracted from carbonates) should record the soil carbonate precipitation temperature (22). Carbonate $\delta^{18}\text{O}$ values and Δ_{47} temperature estimates decrease with time (17, 22, 23), suggesting that elevations increased by 2.5 ± 1 km during late Miocene time, consistent with low elevation estimates from fossil leaves.

We supplement these elevation records with δD data from authigenic clays in late Miocene ash deposits in the Callapa section and $\delta^{18}\text{O}$ data from late Oligocene to early Miocene pedogenic carbonates from the Salla and Huayllapucara/Totora Formations (16) (Figs. 1 and 2 and tables S4 and S6). One challenge in interpreting stable isotope records of elevation is that they can be biased toward lower elevation estimates (i.e., more positive values) by increased surface-water evaporation associated with climate change. δD data of authigenic clay minerals in combination with the oxygen isotope carbonate record ($\delta^{18}\text{O}_\text{c}$) provide a qualitative assessment of this bias because of the retention and fractionation behavior of hydrogen and oxygen in soil and lake water during evaporation (24). δD values of smectite from volcanic ashes of the Callapa Formation parallel $\delta^{18}\text{O}_\text{c}$ values (Fig. 2) and decrease by about 10 to 20 ‰ during the late Miocene. Despite increasingly arid climate, the combined $\delta^{18}\text{O}_\text{c}$ and δD data show trends toward more negative isotopic compositions of meteoric water, supporting the inference that the decrease in $\delta^{18}\text{O}_\text{c}$ reflects a change in surface elevation of the Bolivian Altiplano.

Before the late Miocene, $\delta^{18}\text{O}_\text{c}$ values and paleotemperature estimates suggest a long history of fairly stable surface temperatures and isotopic compositions of surface waters (Fig. 2), perhaps reflecting minimal surface elevation change between ~25 and 10 Ma. Using the paleotemperature estimates from an early middle Miocene fossil-leaf assemblage (21), we converted the $\delta^{18}\text{O}_\text{c}$ values of late Oligocene to early Miocene soil carbonates to surface-water values ($\delta^{18}\text{O}_\text{w}$) (25). For the modern isotopic lapse rate of $h = 472.5\delta^{18}\text{O}_{\text{rainfall}} - 2645$ [where h = elevation in meters (17)], paleoelevation is $<2.3 \pm 1$ km (26) between 10 and 25 Ma, broadly consistent with fossil-leaf estimates (20) (Fig. 4). Before 25 Ma, the only paleoelevation estimates come from paleosol carbonates of the Salla Formation. Both high $\delta^{18}\text{O}_\text{c}$ values and high paleotemperature estimates, based on Δ_{47} values (table S5), suggest elevations close to sea level. [Assuming modern temperature and $\delta^{18}\text{O}$ lapse rates, reconstructed $\delta^{18}\text{O}_\text{w}$ are similar to modern values in the Amazon foreland, and temperatures are slightly warmer than those in the foreland (Fig. 4).] The relatively positive late Oligocene to early Miocene $\delta^{18}\text{O}_\text{c}$ values cannot be explained by diagenesis of carbonate because both higher temperatures and/or diagenesis in the presence of later fluids should produce more negative $\delta^{18}\text{O}_\text{c}$ values (27), which are not observed. In addition, Δ_{47} values suggest reasonable temperatures for surface environments, as opposed to the higher temperatures that might result from burial diagenesis.

The $\delta^{18}\text{O}_\text{c}$, Δ_{47} , and δD compilation (Figs. 2 and 4) suggests that there was at least one discrete

pulse of rapid surface uplift of ~1.5 to 3.5 km (2.5 ± 1 km) between ~10 and 6 Ma and perhaps an earlier phase of surface uplift at ~25 Ma. However, limited data between 30 and 20 Ma preclude an understanding of the nature and extent of the older event. In the following discussion, we review geologic histories of the magmatism, shortening, and incision within the central Andean plateau that, when viewed with sedimentation rates and surface uplift history, shed light on the regional geodynamic processes that induced late Miocene surface uplift.

Magmatism and Distribution of Shortening

Widespread felsic magmatism in the Andean plateau began between 18°S and 24°S at ~25 Ma (28) and has been attributed to steepening of the subducting Nazca slab (29). Despite its wide extent, the volume of pre-late Miocene magmatism was small. Most activity (>85%) between 19°S and 23.5°S occurred between ~8.5 and 4 Ma (30, 31). Mafic lavas erupted throughout the northern and central Altiplano beginning at ~7.5 to 5.5 Ma (32, 33) and at ~7 to 3 Ma in the southern Altiplano and Puna (13, 34) (Fig. 5D). One group of lavas that erupted between 25°S and 26.5°S shows trace element and radiogenic isotopic compositions characteristic of an asthenospheric source, inferred to reflect the removal of eclogitic lower crust and mantle lithosphere beneath the southern Altiplano and Puna plateaus (34).

From 30 to 10 Ma, the Andean plateau experienced east-to-west shortening by ~6 to 12 mm/year across the plateau (3, 5). From 10 to 7 Ma, while elevation increased, shortening ceased and deformation propagated eastward into the Subandean zone (4, 35) (Fig. 5C). This shift in the locus of shortening is consistent with surface uplift, which should decrease the horizontal deviatoric compressive stress under the plateau while applying greater force per unit length to the surrounding lowland.

Geomorphology

Changes in the relief structure of the Plateau also imply that surface uplift occurred since ~10 Ma (36–38). Paleosurfaces on both the eastern slope of the Eastern Cordillera (36, 37) and the western slope of the Western Cordillera (38–43) reflect remnants of low-relief drainage systems that were

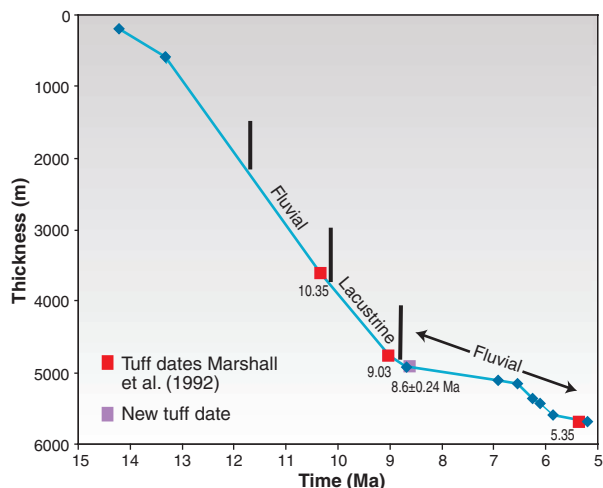


Fig. 3. Sediment thickness (nondecompact) versus time for deposition in eastern limb of the Corque syncline. Stratigraphic thickness versus age in rocks older than 10.35 My come from (57). Constraints on geologic time are indicated by different symbols: red squares are dates from (58), the purple square is the new tuff age reported here (16), and blue diamonds are revised magnetostratigraphy (16). The blue line reflects the rate of sediment accumulation and changes in depositional environment are labeled accordingly. Note the marked decrease in accumulation rates after 9 Ma associated with a change from lacustrine to fluvial deposition.

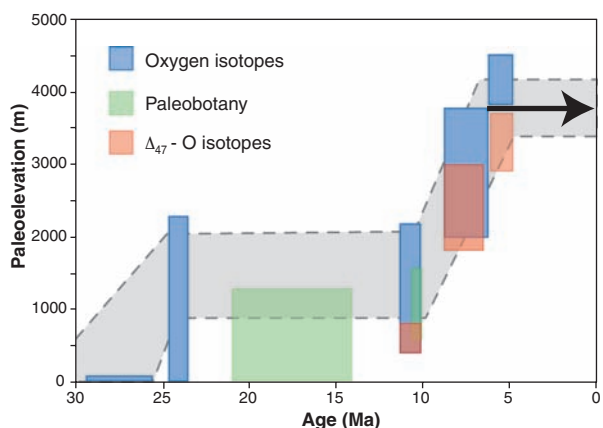


Fig. 4. Multiple proxies of elevation versus time for the central Andean plateau over the past 30 My. Paleoelevation estimates are derived from oxygen isotopes (17, 23), both Δ_{47} and oxygen isotopes (17, 22), and fossil-leaf physiognomy (20, 21).

active between ~7 and 12 Ma in the Eastern Cordillera (36, 37) and until ~10 Ma on the western slope (44). Widespread incision of the paleosurfaces in the Eastern Cordillera began by ~6.5 Ma (37) and in the Western slope began between ~9 and 5.5 Ma (40, 42, 43). Cooling ages of minerals in the Eastern Cordillera also imply that rapid incision began between ~15 and 6 Ma in the absence of substantial shortening (45, 46). Reconstructions of the relief in these incised valleys suggest ~2 km of surface uplift of the Eastern Cordillera (47) and ~1 to 2.5 km of surface uplift of the Western Cordillera (40–42). The western slope of the Andes (north of ~30°S) has had an arid-hyperarid climate since at least 15 Ma (48–50), indicative of atmospheric circulation patterns similar

to the modern pattern, in which rainfall is derived predominantly from the east. Despite dramatically different climates between west and east, the similar timing of incision on the western and eastern slopes supports the notion that incision was induced by surface uplift and rotation of the slopes.

The widespread extent of incision implies that the entire width of the mountain belt—over at least 5° latitude—rose (Fig. 1A) (51). The regional late Miocene paleotopography can be reconstructed using surface uplift estimates in Fig. 4 (for the Altiplano) and the magnitude of relief generated during incision of the Eastern and Western cordilleras (40, 47) (Fig. 1B). There is a large difference in cross-sectional area between the average modern elevation of the paleosurface and the 10-Ma reconstructed topography. For crustal thickening to account for this difference would require shortening rates in excess of 40 mm/year over the 1 to 3 My during which surface uplift occurred. This is four times greater than the observed rates in the Andean plateau over the past 40 My, which seems implausible. Flow of middle-lower crust from the Eastern and Western cordilleras to the Altiplano (52) fails to explain the simultaneous rise of the cordilleras, which should subside or remain the same elevation as lower crustal material flows laterally. We conclude that the rapid rate, magnitude, and regional extent of surface uplift, in addition to crustal thickening, also require a mantle contribution, most likely the isostatic response to removal of eclogite and mantle lithosphere.

Climatic responses to Andean surface uplift may extend beyond South America. For example, the presence of the Andes deflects the Intertropical Convergence Zone to north of the equator in the Pacific, which influences the strength and distribution of monsoonal climates with Pacific teleconnections (53). It is therefore possible that punctuated Andean surface uplift contributed to the reorganization of south Asian climate observed in the late Miocene.

Geodynamic Implications

Crustal thicknesses of 60 to 70 km in the central Andes are the result of protracted shortening and thickening over the past 50 My. Despite extensive crustal thickening, regional reconstruction of paleotopography suggests paleoelevations of <2 km in the Altiplano and 2.5 to 3.5 km in the Eastern and Western cordilleras until ~10 Ma (51). These anomalously low paleoelevations probably reflect the presence of dense eclogitic lower crust, which held the surface down. An analogous region today might be the western Sierras Pampeanas in Argentina, with 60-km-thick crust but average elevations of ~1 km (54).

Geologic observations suggest that the internal structure of the Andean lithosphere changed between ~10 and 6 Ma. During this time, the entire width of the plateau experienced surface uplift, deep incision of low-relief paleosurfaces initiated on the eastern and western slopes of the Andes, sedimentation rates within the Altiplano basin decreased dramatically while the basin

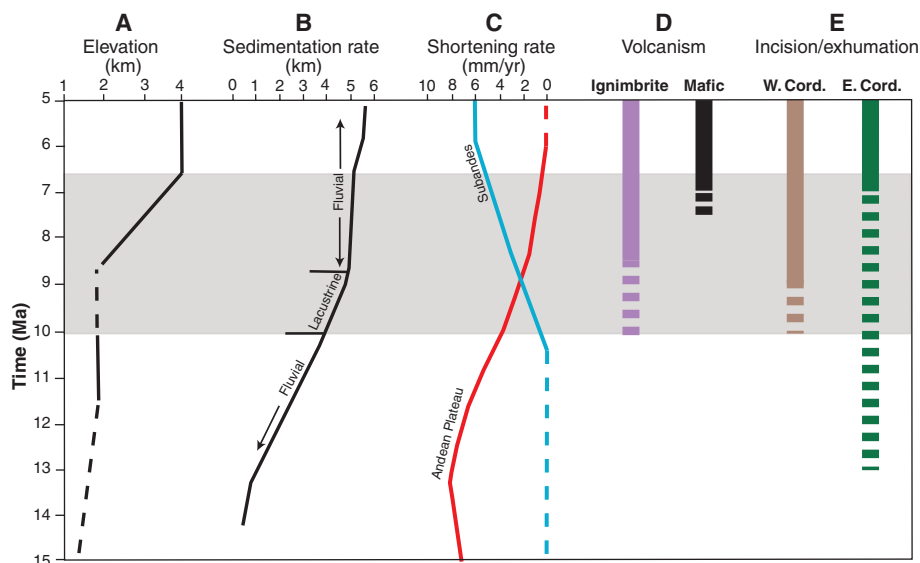


Fig. 5. Synthesis of geologic events that occurred in the central Andean plateau between $\sim 17^{\circ}\text{S}$ and 26°S latitude during the middle to late Miocene. **(A)** Elevation history based on the various proxies in Fig. 4. **(B)** Subsidence rate for the sediments exposed in the Corque syncline (Fig. 3). **(C)** Cumulative shortening rates for the Andean plateau (5) and Subandean range (4). **(D)** Volcanic activity (12, 31). **(E)** Incision and exhumation of the eastern (36, 37, 45, 46) and western flanks (40, 42, 43) of the central Andean plateau.

transitioned from underfilled lacustrine environments to filled fluvial/floodplain environments, shortening ceased in the plateau and propagated into the foreland, and widespread and voluminous ignimbrite eruption began, followed closely in time by mafic volcanism (Fig. 5). Together, these observations are best explained by the removal of dense eclogite and mantle lithosphere, triggering regional surface uplift of ~ 1.5 to 2.5 km. The amount of surface uplift requires the removal of eclogite and mantle lithosphere of ~ 80 to 140 km thick, an amount that fits within the geometry of the subduction zone (51). Removal by drips of downward-flowing lower lithosphere can explain the sedimentation history in the Altiplano in that the region above the drip should experience rapid subsidence during drip formation (55), accompanied by rapid rates of sedimentation and underfilled basin conditions. Both rapid sedimentation and underfilled lacustrine conditions are observed in the Altiplano between ~ 13 and 9 Ma, just before the late Miocene surface uplift (Figs. 3 and 5, A and B). We suggest that the morphology of broad, flat, high-elevation, orogenic plateaus is the product of phases of both crustal and mantle lithosphere thickening punctuated by discrete intervals of surface uplift associated with the convective removal of dense lower crust and mantle lithosphere. Between ~ 40 and 10 Ma, crustal shortening, lower crustal flow, and erosion/sedimentation redistributed crustal lithosphere while eclogitic lower crust and mantle lithosphere accumulated at depth. This long-term history created the conditions that resulted in lower lithosphere removal between ~ 10 and 6 Ma. After 6 Ma, continued lower crustal flow and erosion and sedimentation redistributed mass within the crust to enhance the low-relief landscape observed in the plateau today.

References and Notes

1. P. Bird, *J. Geophys. Res.* **83**, 4975 (1978).
2. P. A. England, G. A. Houseman, *J. Geophys. Res.* **94**, 17561 (1989).
3. N. McQuarrie, B. K. Horton, G. Zandt, S. Beck, P. G. DeCelles, *Tectonophysics* **399**, 15 (2005).
4. L. Echavarría, R. Hernandez, R. Allmendinger, J. Reynolds, *Am. Assoc. Pet. Geol. Bull.* **87**, 965 (2003).
5. K. Elger, O. Oncken, J. Glodny, *Tectonics* **24**, TC4020 (2005).
6. S. L. Beck, G. Zandt, *J. Geophys. Res.* **107**, 2230 (2002).
7. P. Wigger *et al.*, in *Tectonics of the Southern Central Andes: Structure and Evolution of an Active Continental Margin*, K. J. Reutter, E. Scheuber, P. J. Wigger, Eds. (Springer, Berlin, 1994), pp. 23–48.
8. C. Dorbath, M. Granet, *Tectonophysics* **259**, 117 (1996).
9. S. C. Myers, S. Beck, G. Zandt, T. Wallace, *J. Geophys. Res.* **103**, 21233 (1998).
10. L. Hoke, D. R. Hilton, S. H. Lamb, K. Hammerschmidt, H. Friedrichsen, *Earth Planet. Sci. Lett.* **128**, 341 (1994).
11. R. W. Kay, S. M. Kay, *Tectonophysics* **219**, 177 (1993).
12. S. M. Kay, C. Mpodozis, B. Coira, in *Geology and Ore Deposits of the Central Andes*, B. J. Skinner, Ed. (Society of Economic Geologists, Littleton, CO, 1999), vol. 7, pp. 27–59.
13. G. A. Houseman, D. P. McKenzie, P. Molnar, *J. Geophys. Res.* **86**, 6115 (1981).
14. W. C. Tao, R. J. O'Connell, *J. Geophys. Res.* **97**, 8877 (1992).
15. D. C. Pope, S. D. Willett, *Geology* **26**, 511 (1998).
16. Supporting online material is available on Science Online.
17. J. Quade, C. Garzzone, J. Eiler, *Rev. Mineral. Geochem.* **66**, 53 (2007).
18. R. W. Allmendinger, T. E. Jordan, S. M. Kay, B. L. Isacks, *Annu. Rev. Earth Planet. Sci.* **25**, 139 (1997).
19. T. Sempere *et al.*, *Geol. Soc. Am. Bull.* **109**, 709 (1997).
20. K. M. Gregory-Wodzicki, *Geol. Soc. Am. Bull.* **112**, 1091 (2000).
21. K. M. Gregory-Wodzicki, K. Velasquez, W. C. MacIntosh, *J. South Am. Earth Sci.* **11**, 533 (1998).
22. P. Ghosh, C. N. Garzzone, J. M. Eiler, *Science* **311**, 511 (2006).
23. C. N. Garzzone, P. Molnar, J. C. Libarkin, B. J. MacFadden, *Earth Planet. Sci. Lett.* **241**, 543 (2006).
24. A. Mulch, C. P. Chamberlain, *Rev. Min. Geochem.* **66**, 89 (2007).
25. S.-T. Kim, J. R. O'Neil, *Geochim. Cosmochim. Acta* **61**, 3461 (1997).
26. Uncertainties are estimated as in (56) by assuming that the modern climate captures the characteristics of the rainout process in the past. Using a bootstrap simulation approach, errors are propagated by incorporating the scatter in empirical data that constrain the $\delta^{18}\text{O}_w$ -versus-altitude gradient, uncertainty of $\pm 5^{\circ}\text{C}$ on the temperature of carbonate precipitation, and scatter in the temperature-dependent ^{18}O fractionation between water and calcite. This yields 1σ errors of ± 500 m at elevations > 4 km, increasing to ± 1000 m at elevations of < 1 km. Assuming a Rayleigh distillation process for fractionation during condensation from a vapor mass, higher-than-modern global temperature in the late Oligocene to late Miocene would lower the $\delta^{18}\text{O}_w$ -versus-altitude gradient, which would cause an underestimation of paleoelevation for distillation from a vapor mass with a similar to modern starting composition (56).
27. C. N. Garzzone, D. L. Dettman, B. K. Horton, *Palaeogeogr. Palaeoclimatol. Palaeoecol.* **212**, 119 (2004).
28. B. L. Isacks, *J. Geophys. Res.* **93**, 3211 (1988).
29. D. E. James, I. S. Sacks, B. J. Skinner, in *Geology and Ore Deposits of the Central Andes*, B. J. Skinner, Ed. (Society of Economic Geologists, Littleton, CO, 1999), vol. 7, pp. 1–25.
30. M. C. W. Baker, P. W. Francis, *Earth Planet. Sci. Lett.* **41**, 175 (1978).
31. S. L. de Silva, W. D. Gosnold, *J. Volcanol. Geotherm. Res.* **167**, 320 (2007).
32. S. Lamb, L. Hoke, *Tectonics* **16**, 623 (1997).
33. G. Carlier *et al.*, *Geology* **33**, 601 (2005).
34. S. M. Kay, B. Coira, J. Viramonte, *J. Geophys. Res.* **99**, 24323 (1994).
35. I. Moretti, P. Baby, M. E. D. Zubieta, *Petrol. Geosci.* **2**, 17 (1996).
36. T. L. Gubbels, B. L. Isacks, E. Farrar, *Geology* **21**, 695 (1993).
37. L. Kennan, S. H. Lamb, L. Hoke, in *Palaeosurfaces; Recognition, Reconstruction and Palaeoenvironmental Interpretation*, M. Widdowson, Ed. (Geological Society of London, London, 1997), vol. 120, pp. 307–323.
38. M. Farías, R. Charrier, D. Comte, J. Martinod, G. Hérail, *Tectonics* **24**, TC4001 (2005).
39. M. García, G. Hérail, *Geomorphology* **65**, 279 (2005).
40. G. D. Hoke *et al.*, *Tectonics* **26**, TC5021 (2007).
41. F. Kober, F. Schlunegger, G. Zeilinger, H. Schneider, in *Tectonics, Climate and Landscape Evolution*, S. D. Willett, N. Hovius, M. T. Brandon, D. M. Fisher, Eds. (Geological Society of America, Denver, CO, 2006), pp. 75–86.
42. T. F. Schildgen, K. V. Hodges, K. Whipple, P. W. Reiners, M. S. Pringle, *Geology* **35**, 523 (2007).
43. J.-C. Thouret *et al.*, *Earth Planet. Sci. Lett.* **263**, 151 (2007).
44. G. D. Hoke, B. L. Isacks, T. E. Jordan, J. S. Yu, *Geology* **32**, 605 (2004).
45. J. B. Barnes, T. A. Ehlers, N. McQuarrie, P. B. O'Sullivan, J. D. Pelletier, *Earth Planet. Sci. Lett.* **248**, 118 (2006).
46. R. J. Gillis, B. K. Horton, M. Grove, *Tectonics* **26**, (2006); 10.1029/2005TC001887.
47. R. Barke, S. Lamb, *Earth Planet. Sci. Lett.* **249**, 350 (2006).
48. J. Houston, A. J. Hartley, *Int. J. Climatol.* **23**, 1453 (2003).
49. C. N. Alpers, G. H. Brimhall, *Geol. Soc. Am. Bull.* **100**, 1640 (1988).
50. J. A. Rech, B. S. Currie, G. Michalski, A. M. Cowan, *Geology* **34**, 761 (2006).
51. G. D. Hoke, C. N. Garzzone, *Earth Planet. Sci. Lett.*, published online 22 April 2008; 10.1016/j.epsl.2008.04.008.
52. L. Husson, T. Sempere, *Geophys. Res. Lett.* **30**, 1243 (2003).
53. K. Takahashi, D. S. Battisti, *J. Clim.* **20**, 3434 (2007).
54. H. Gilbert, S. Beck, G. Zandt, *Geophys. J. Int.* **165**, 383 (2006).
55. G. A. Houseman, E. A. Neil, M. D. Kohler, *J. Geophys. Res.* **105**, 16237 (2000).
56. D. B. Rowley, C. N. Garzzone, *Annu. Rev. Earth Planet. Sci.* **35**, 463 (2007).
57. P. Roperch, G. Hérail, M. Forani, *J. Geophys. Res.* **104**, 20415 (1999).
58. L. G. Marshall, C. C. Swisher III, A. Lavenu, R. Hoffstetter, G. H. Curtis, *J. South Am. Earth Sci.* **5**, 1 (1992).
59. We thank D. Foster for $^{40}\text{Ar}/^{39}\text{Ar}$ analyses and R. Allmendinger and P. Molnar for suggestions that improved the paper. This work was supported by NSF EAR grants 0230232 and 0635678 (to C.N.G.) and 0350396 (to J.C.L.).

Supporting Online Material

www.sciencemag.org/cgi/content/full/320/5881/1304/DC1
Materials and Methods

SOM Text

Figs. S1 to S4

Tables S1 to S6

References

27 September 2007; accepted 18 March 2008
10.1126/science.1148615